


Multiscale Comparative Evaluation of the GPM and TRMM Precipitation Products Against Ground Precipitation Observations Over Chinese Tibetan Plateau

Qiong Li , Jiahua Wei , Jianguo Yin, Zhen Qiao, Wang Peng, and Haiyue Peng

Abstract—This study aims to evaluate the performances of two latest released global precipitation measurement (GPM)-era satellite precipitation final run products (integrated merged multisatellite retrievals IMERG-V06B and Global Satellite Mapping of Precipitation GSMaP-V07) and one tropical rainfall measuring mission (TRMM)-era product (TMPA-3B42-V07) at hourly, daily, and monthly scale over the Tibetan plateau (TP), with special focus on the performances at different rain intensities, subbasins, and elevations at daily scales. Besides, hourly scale evaluations were carried out for one grid box value of IMERG-V06B and GSMaP-V07 versus 15 rain gauges on the rainy season, 2019. Results indicated that: First, GSMaP-V07 outperformed TMPA-3B42-V07 and IMERG-V06B with higher correlation coefficient and lower relative bias, mean absolute error, and root-mean-squared error values at daily and monthly scale. Second, satellite products showed overestimation during light rain and underestimation throughout moderate rain, heavy rain, and rainstorm; Third, satellite products have performed relatively better in lower elevation (<3000 m) regions, but they greatly overestimated the precipitation (more than 50%) at high-elevation (>4000 m). Fourth, satellite precipitation products performed better in the source region of the Yellow River, Yangtze River, Lancang River, and Nujiang River basins, whereas the products greatly overestimated the precipitation in the source region of the Yarlung zangbo River basin. In arid climate regions (Qiangtang Basin and Qaidam Basin), GSMaP-V07 had better performances than other products; and finally, although GSMaP-V07 showed higher overestimation than IMERG-V06B product at hourly scale, it has better consistency with rain-gauge

observations. For satellite precipitation data application within the TP, we recommend the GSMaP-V07 over the IMERG-V06B. Furthermore, improvement on the multisatellite rainfall retrieval algorithm is required.

Index Terms—Global Satellite Mapping of Precipitation (GSMaP), integrated merged multisatellite retrievals (IMERG), satellite precipitation products, Tibetan plateau (TP), TMPA.

I. INTRODUCTION

THE Tibetan plateau (TP) is located in central Asia and has an average elevation of about 4000 m (above sea level) and an area of approximately 2.5 million km² [1]. The TP is China's largest and the world's highest highland, which is well known as the “Third Pole”. The TP plays a crucial role in the Asian monsoon system and for atmospheric circulation at the hemispheric scale through thermal and orographic forcing [2], [3]. Present atmospheric circulation patterns over the TP and surroundings are under the combined and competitive influences of the East Asian and South Asian monsoons and the westerlies [4]. Precipitation is a vital hydrometeorological variable that plays a key role in the hydrological cycle, the energy balance of the earth as well as in the ecological environments [5]. Rainfall and snowmelt dominate the hydrological budget of the TP [6], but the paucity of meteorological data, especially precipitation, limits the in-depth understanding of the water cycle over the TP.

Precipitation measurement over a variety of spatial and temporal scales has always been a challenging topic in the past decade. To date, there are three dominating methods to measure precipitation, which include rain gauges, weather radars, and satellite remote sensing. Rain gauges provide the most accurate and direct physical measurement of precipitation at the point scale [7]. Generally, interpolation algorithms such as the Thiessen polygon, inverse distance weighting methods, MicroMet [8] and precipitation lapse (PrecLaps) algorithms have been typically used together with rain-gauge measurements to derive spatially distributed precipitation [9]–[11]. The performances of the interpolation algorithms mainly depend on the gauge density and the topographic features. Over the TP, the rain gauges are scarce (0.6/10000 km² at most) and unevenly distributed [12], [13], consequently, the interpolation algorithms have obvious lower performances at the regional scale. Besides

Manuscript received June 21, 2020; revised October 5, 2020 and November 12, 2020; accepted December 12, 2020. Date of publication December 29, 2020; date of current version February 12, 2021. This work was supported in part by the National key research and development project under Grants 2017YFC0403600, and 2016YFE0201900, in part by the National Natural Science Foundation of China under Grants 91847302, 51909130, in part by the National Natural Science Foundation of Technology Department of Qinghai Province under Grant 2019-ZJ-968Q, and in part by the State Key Laboratory of Hydro-science and Engineering under Grant sklhse-2020-low01. (Corresponding author: Jiahua Wei.)

Qiong Li, Zhen Qiao, Wang Peng, and Haiyue Peng are with the State Key Laboratory of Plateau Ecology and Agriculture, Qinghai University, Xining 810016, China (e-mail: liqiong1118@126.com; 584851559@qq.com; 937248117@qq.com; 1502989456@qq.com).

Jiahua Wei is with the State Key Laboratory of Plateau Ecology and Agriculture, Qinghai University, Xining 810016, China, and also with the State Key Laboratory of Hydroscience and Engineering, Tsinghua University, Beijing 100084, China (e-mail: weijiahua@tsinghua.edu.cn).

Jianguo Yin is with the Key Laboratory of Petroleum Resources, Gansu Province, Northwest Institute of Eco-Environment and Resources, Chinese Academy of Sciences, Lanzhou 730000, China (e-mail: jianguoyin@lzb.ac.cn).

Digital Object Identifier 10.1109/JSTARS.2020.3047897

rain-gauge, weather radar can also observe the internal structure of precipitation and obtain real-time rainfall data with high temporal and spatial resolutions over large areas [14]. Moreover, radars may have difficulty to cover the whole region in mountain area, because the mountains can block the signals [15], [16]. The satellite remote sensing can obtain high spatio-temporal resolution precipitation measurements at regional and global scales [17]–[19]. Therefore, satellite remote sensing has emerged as a promising approach for research and application over the TP.

In recent years, many quasi-global and high spatio-temporal resolution satellite precipitation datasets have been produced. These datasets include the Tropical Rainfall Measuring Mission (TRMM) multisatellite precipitation analysis (TMPA) [20], Climate Prediction Center MORPHing technique [21], Precipitation estimation from remotely sensed information using artificial neural networks (PERSIANN) [22], Global Satellite Mapping of Precipitation (GSMaP) [23], and integrated multisatellite retrievals for global precipitation measurement GPM (GPM-IMERG) [17]. Previous studies have found that the latest version of TMPA precipitation product outperforms other satellite products in many regions around the world in terms of lower errors and biases [14], [24], [25]; however, it has inherent flaws in measuring solid or light precipitation over higher latitudes and altitudes [14], [17], [19], [20].

As a successor for the TRMM, which was launched in November 1997, the GPM core observatory (launched in February 2014) marked a transition from the TRMM to the GPM era. The GPM core observatory consists of a dual-frequency precipitation radar (DPR) and a GPM microwave imager (GMI) with enhanced capabilities to measure light rain (less than 0.5 mm/hour) and solid precipitation [26]. The GPM mission has two rainfall products, Level-3 IMERG (the Integrated Merged Multi-satellite Retrievals) and GPM-era GSMaP, provided separately by the American National Aeronautics and Space Administration (NASA) and the Japanese Aerospace Exploration Agency (JAXA).

IMERG had better performance than TMPA-3B42-V7 at both subdaily and daily time scales in almost every subregion of mainland China [27], United States (US) [28], Africa [29], Central Amazon [30], Iran [31], and in the Mekong River basin [32]. For hydrological utility, the Day-1 IMERG outperformed TMPA products during the forcing of the coupled routing and excess storage hydrological model to simulate streamflow at a daily scale in Ganjiang River basin [33]. The GSMaP-gauge (gauge-adjusted GSMaP) performed slightly better than IMERG-C (gauge-calibrated IMERG) during the forcing of the variable infiltration capacity (VIC) model in the source region of the Yellow River (SRYR) [34]. Summarily, the IMERG and GSMaP considerably performed better than TMPA, showing GPM as a good successor of the TRMM product.

Nonetheless, the GPM IMERG and GSMaP datasets have not been widely and thoroughly validated in regions having complex topography, especially high elevation areas such as the TP. Xu *et al.* [12] evaluated the performances of GPM-IMERG-V5 and TMPA-3B42-V7 products based on a high-density network of rain gauges over southern TP during the rainy season of

2014 (May to October), and found that GPM showed better detecting ability for light rainfall (0–5 mm/d) events but there is no detection skill for both GPM and TRMM at high-elevation regions (>4500 m). Previous studies [12], [27], [35] have found that IMERG product overestimates maximum rainfall intensity within the TP and besides, the evaluation of IMERG product at elevations below 3500 m was much better than those above 3500 m. Currently, the evaluation and comparison of these products have only been performed for less than two years, which cannot reflect seasonal error distribution. Besides, few researchers have assessed the accuracy of the latest version of the GPM-era products over the TP. In addition, previous researchers evaluated the performances of IMERG and GSMaP products over the TP only at regional scale but not at the basin scales [34], [36], [37], which might notably influence their applications during hydrological modeling and extreme weather impact assessment.

Satellite precipitation products are the most basic and important data sources over regions with sparse meteorological stations such as the TP. Since there are few stations in the hinterland of the TP; therefore, the satellite precipitation products remain the only source of precipitation observation. Hence, it is very important to evaluate the accuracy and regional applicability of satellite precipitation products. We evaluated the performances of the TRMM (TMPA-3B42-V07) and the newest GPM (GPM-IMERG-V06B and GPM-GSMaP-V07) era rainfall products from 2015 to 2019 by considering rainfall intensities, elevation effect, and different river basin over the TP region. Most importantly, we conducted a two-month trial rainfall monitoring in one grid box of IMERG-V06B and GSMaP-V07 with 15 rain-gauges. It is worth mentioning that the density of the rain-gauge networks (15/100 km²) used for evaluation in this study was by far the highest over the TP. Our evaluation will be based on the “final” run products, which are corrected by NOAA CPC global rain gauge data.

The article is organized as follows. The regional characteristics of the study area, data sources, and various statistics for validating satellite rainfall products against rain gauges are presented in Section II. The performances of the GPM and TRMM era products based on geographical effect, rain intensities, different river basins, are analyzed and discussed in Section III. The discussions are presented in section IV. Lastly, key summary and conclusion are presented in Section V.

II. MATERIALS AND METHODS

A. Study Area

Known as the “Asian water tower”, the TP is the source of major Asian rivers, such as the Yellow, Yangtze, Lancang (Mekong), Nujiang (Salween), Indus, and Yarlung-zangbo (Brahmaputra-Ganges) river (Fig. 1). The TP region is dominated by the Plateau mountain climate, characterized by complex topography and high elevation, and showing great precipitation variability. The average annual rainfall ranges from about 1500 to 100 mm with an obvious southeast to northwest gradient. The TP has an average annual temperature below 0 °C and approximately 130–140 frost-free days.

TABLE I
CHARACTERISTICS OF SATELLITE PRECIPITATION PRODUCTS

Name	Temporal resolution	Spatial resolution	Coverage	Dates period	Correction
GPM-IMERG-V06B	0.5 hourly	0.1°	60°N-S	2000.6 - present	GPCC monthly data
GPM-GSMaP Gauge -V07	1 hourly	0.1°	60°N-S	2014.3 - present	CPC daily data
TMPA-3B42-V07	3 hourly	0.25°	50°N-S	1998.1 - 2019.12	GPCC monthly data

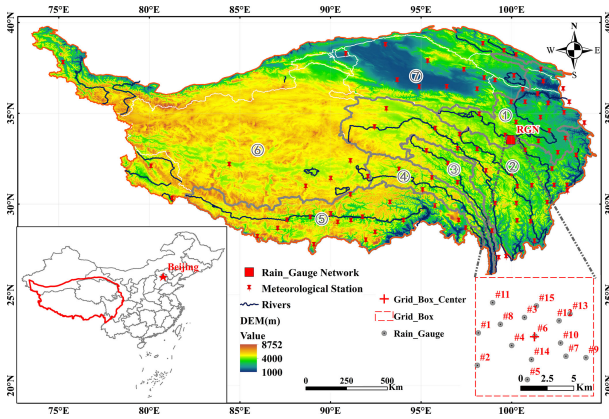


Fig. 1. Geographical map of the study location showing the digital elevation model (DEM), distribution of rain-gauges, and river basins within the TP. The source region of the ① Yellow River (SRYR); ② Yangtze River (SRYZR); ③ Lancang River (SRLCR); ④ Nujiang River (SRNR); ⑤ Yarlung zangbo River (SRYLZB); ⑥ Qiangtang Basin (QTB); ⑦ Qaidam Basin (QDMB).

B. Ground Gauge Data

The rain gauge network used for validation comprises 91 meteorological stations over the TP and are maintained by the China Meteorological Administration. A high-density network of rain gauges (15 tipping-bucket rain gauges installed in one GPM grid box) is established in the SRYR. The layout of these rain gauges is shown in Fig. 1. The red dots represent the 91 meteorological stations while the red square is where the high-density network of rain-gauges is located.

Daily precipitation from the 91 meteorological stations are available in the SURF CLI MUL DAY V3.0 dataset¹ and are retrieved from 2015 through 2019. These datasets were compiled by the National Meteorological Information Center and subjected to a series of quality controls.

Hourly precipitation from 15 tipping-bucket rain gauges is available from August 1, 2019 to September 30, 2019. Although *in-situ* observation of precipitation is only two months of the rainy season and all rain gauges are in one GPM grid box, it is useful to evaluate the subhourly performances of the GPM products and estimate whether the spatial resolution of the remote sensing precipitation products could satisfy the research demand in the complex mountain area.

C. Satellite Precipitation Product

The characteristics of TMPA, GPM-IMERG, and GPM-GSMaP products used in this study are described in Table I.

¹[Online]. Available: <http://data.cma.cn/>

For daily and monthly scale evaluation, the IMERG, GSMaP, TMPA daily scale data from January 2015 to December 2019 were used, while for hourly scale evaluation, the IMERG and GSMaP hourly scale data of the grid box in SRYR from August 1, 2019 to September 30, 2019 were employed for the analysis over the TP.

IMERG is a level 3 multisatellite precipitation algorithm of GPM, which combines all available microwave precipitation estimates, infrared (IR) satellite estimates, and monthly gauge precipitation data. The calibrated IMERG final run product provides more accurate precipitation because it is adjusted by GPCC monthly gauge data [38]. The GPM IMERG final run version 06B product (first released to the public since August, 2019) is the latest level-3 GPM precipitation dataset and is used in the current study.

GPM-GSMaP was developed in Japan toward the GPM mission and it combines various available microwave and infrared sensors, intending to develop high-precision precipitation products. The GSMaP-gauge is a gauge-calibrated product that adjusts the GSMaP-MVK estimate with NOAA/CPC gauge-based analysis of global daily precipitation [39]. The latest released GSMaP-gauged V07 daily and hourly scales data are used in the study.

TMPA is one of the TRMM precipitation measurement products combined from multiple satellites and calibrated IR data. The TMPA data products adjusted with GPCC monthly precipitation gauge data and ensures that the 3-hourly averages in 3B42 sum to the monthly totals in 3B43 [20]. The TRMM launched on November 1997 is a joint space mission between NASA and JAXA and has been widely used in hydrometeorological research during the past decade. The data used in this study are TMPA-3B42-V07 daily data over the TP. As the long-record IMERG products are now available, the TMPA and TMPA-RT products have ended up on December 31, 2019.

The TMPA, GPM-IMERG, GPM-GSMaP products used in this study are calibrated by CPC daily or GPCC monthly data. The data of 194 China's International Exchange Stations are used in CPC and GPCC dataset production, 23 of which are distributed over the TP. Considering that 91 stations over the TP are used to evaluation and comparison, about 75% gauge stations are independent.

D. Methodology

To quantitatively compare GPM-era (IMERG and GSMaP) and TRMM-era (TMPA-3B42) precipitation products, several widely used statistical metrics were applied in this study. The

TABLE II
EQUATIONS OF THE INDICATORS

Statistic metrics	Equations	Unit	Perfect value
CC	$CC = \frac{\sum_{i=1}^n (G_i - \bar{G}) (S_i - \bar{S})}{\sqrt{\sum_{i=1}^n (G_i - \bar{G})^2} * \sqrt{\sum_{i=1}^n (S_i - \bar{S})^2}}$	—	1
RBias	$RB = \frac{\sum_{i=1}^n (S_i - G_i)}{\sum_{i=1}^n G_i}$	%	0
RMSE	$RMSE = \sqrt{\frac{1}{n} \sum_{i=1}^n (S_i - G_i)^2}$	mm	0
MAE	$MAE = \frac{1}{n} \sum_{i=1}^n S_i - G_i $	mm	0
POD	$POD = \frac{H}{H + M}$	—	1
FAR	$FAR = \frac{F}{H + F}$	—	0
CSI	$CSI = \frac{H}{H + M + F}$	—	1
ETS	$ETS = \frac{H - H_e}{H + M + F - H_e}$ $H_e = \frac{(H + M)(H + F)}{n}$	—	1

equations and perfect values of these metrics are listed in Table II. The correlation coefficient (CC) describes the agreement between the satellite and gauge precipitation observations. If there is no linear correlation or a weak linear correlation, CC is close to zero. The relative bias (RBias) describes the systematic bias of satellite precipitation products. A positive bias indicates an overestimation while a negative bias means an underestimation of the satellite precipitation. The root-mean-squared error (RMSE) corresponds to the square root of the average of the squared differences between the estimates and the observed rainfall and is used to measure the average error magnitude. RMSE gives greater weight to larger errors relative to the mean absolute error (MAE). The MAE is chosen to measure the average difference between the satellite estimates and gauge observations.

The probability of detection (POD), false alarm rate (FAR), frequency bias index (FBI), critical success index (CSI), and equitable threat score (ETS) were calculated at daily and sub-daily scale to quantitatively examine the detection capabilities in rain events of satellite estimates. POD measures the fraction of occurred precipitation events that are correctly detected by

satellite products. FAR measures the fraction of events in which satellite detects precipitation but precipitation does not occur. FBI is the ratio of the frequency of satellite estimates to the frequency of gauge-based precipitation. It ranges from 0 to ∞ with an optimum value of 1. FBI greater than 1 shows an overestimation while FBI less than 1 presents an underestimation in rainfall detected from satellite estimates as compared to gauge-based observations. CSI gives the overall fraction of events that are correctly diagnosed by satellite estimates. ETS answers the question of how well the satellite estimated precipitation events correspond to the gauge observed precipitation events.

where N is the number of samples; G_i and \bar{G} stand for individual and averaged gauged observation; S_i and \bar{S} indicate individual and averaged satellite precipitation estimation; Contingency table metrics in Table III is used to calculate H , F , and M . H represents the observed rain by gauge, which is detected by satellite correctly, F is not the observed rain but detected falsely, whereas M is the observed rain not detected. The rain and no rain thresholds are set to 0.1 mm for both hourly and daily scales.

TABLE III
CONTINGENCY TABLE SHOWS HOW THE FOUR EVENTS ARE IDENTIFIED BY SATELLITE PRECIPITATION AND RAIN GAUGE PRECIPITATION

Satellite product	Rain Gauge		
		Rain($\geq 0.1\text{ mm/h}$)	No rain($<0.1\text{ mm/h}$)
	Rain($\geq 0.1\text{ mm/h}$)	Hit(H)	False(F)
	No rain($<0.1\text{ mm/h}$)	Miss(M)	Non event

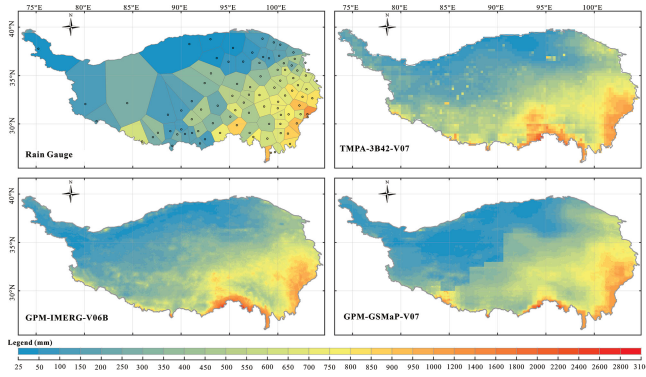


Fig. 2. Spatial distributions of mean annual precipitation for rain-gauges, TMPA-3B42-V07, IMERG-V06B, and GSMaP-V07 from 2015 to 2019 over the TP.

Probability density function is used for comparing the characteristics of different precipitation datasets in terms of precipitation intensity and estimation sensitivity [40]. Probability density function by occurrence (PDFo) and Probability density function by volume (PDFv) are used to describe rainfall distributions from the perspectives of frequency and volumes, respectively. PDFo is computed as the ratio of the number of rain events under different rainfall intensities to the total number of rain events, whereas PDFv is estimated as the ratio of the relative volumetric contribution of the rain rates under different rainfall intensities to the total rainfall volume.

Taylor diagrams are plotted to graphically summarize how well the three different precipitation estimation matches the gauge observations in terms of CC, standard deviation, and centered RMSE. Each point in the 2-D Taylor diagram can represents the three statistics simultaneously that are related by a formula similar to the law of cosine [41]. On the Taylor diagram, the radial coordinate is the magnitude of the normalized standard deviation while the uneven angular coordinate denotes the CC. The closer the marker gets to the observation, the better the precipitation product performs.

III. RESULTS

A. Similarity of Spatial Rainfall Patterns

The spatial distribution of mean annual precipitation for rain gauges, TMPA, IMERG, and GSMaP are shown in Fig. 2. Over the TP, the mean precipitation rate for rain gauges calculated by the Thiessen polygon method was 0.86 mm/d. The mean precipitation rates for TMPA, IMERG, and GSMaP were 1.2, 1.09, and

1.05 mm/d, which were about 39.53%, 26.74%, 22.09% higher than rain gauges mean precipitation, respectively.

All products showed a decreasing trend from the southeast to the northwest, which are generally consistent with rain gauges precipitation. The maximum rainfall occurred in the Himalayan region with mean annual precipitation of more than 2000 mm for satellite precipitation products, but the rain gauges precipitation in this area were about 1200 mm. Lower precipitation occurred in the west and north of the TP (Qiangtang Basin (QTB) and Qaidam Basin (QDMB)), where the Westerlies do not prevail and the Indian monsoon was relatively weak during the warm period [41].

B. Statistical Performance of Satellite Precipitation Estimates

1) *Probability Density Function of Precipitation Intensity:* Fig. 3 shows the PDFo and PDFv for TMPA-3B42-V07, IMERG-V06B and GSMaP-V07 at a daily scale with different precipitation intensities over the TP. The smallest threshold to measure the precipitation is 0.1 mm, so the rain in the bin 0.1~1 mm represents no rain events. The bin 0~0.1 mm/d of daily PDFo was displayed separately in the top right corner of Fig. 3(a) because most precipitation (more than 60%) falls in the bin 0~0.1 mm/d representing no rain events. On the daily scale, TMPA-3B42-V07 demonstrated better ability in capturing light precipitation events (0.1~10 mm/d) than IMERG-V06B and GSMaP-V07 however TMPA-3B42-V07 showed an underestimation in the rainfall volume of light rainfall (0.1~10 mm/d). For moderate and heavy rainfall (10~50 mm/d), TMPA-3B42-V07 appears to have more precipitation than rain gauges observation and showed an overestimation in the rainfall volume.

IMERG-V06B showed obvious overestimation in light rainfall (0.1~10 mm/d) considering PDFo and PDFv. IMERG-V06B produced more precipitation than rain gauge observations in light rainfall and showed an overestimation. As for moderate and heavy rainfall (10~50 mm/d), GSMaP-V07 had less precipitation than rain gauges observation and showed an underestimation in rainfall volume. For heavy rainfall (25~50 mm/d) and rainstorm (50~100 mm/d), TMPA-3B42-V07 and IMERG-V06B had more precipitation than rain gauges observations and showed an overestimation in rainfall volume. Overall, TMPA-3B42-V07, IMERG-V06B, and GSMaP-V07 products overestimated the total precipitation volume.

2) *Statistical Evaluation of Satellite Products:* Fig. 4 displays the spatial distributions of selected evaluation metrics (CC, RBais, MAE, RMSE, POD, FAR, CSI, and ETS) for the daily TMPA-3B42-V07, IMERG-V06B, and GSMaP-V07 data

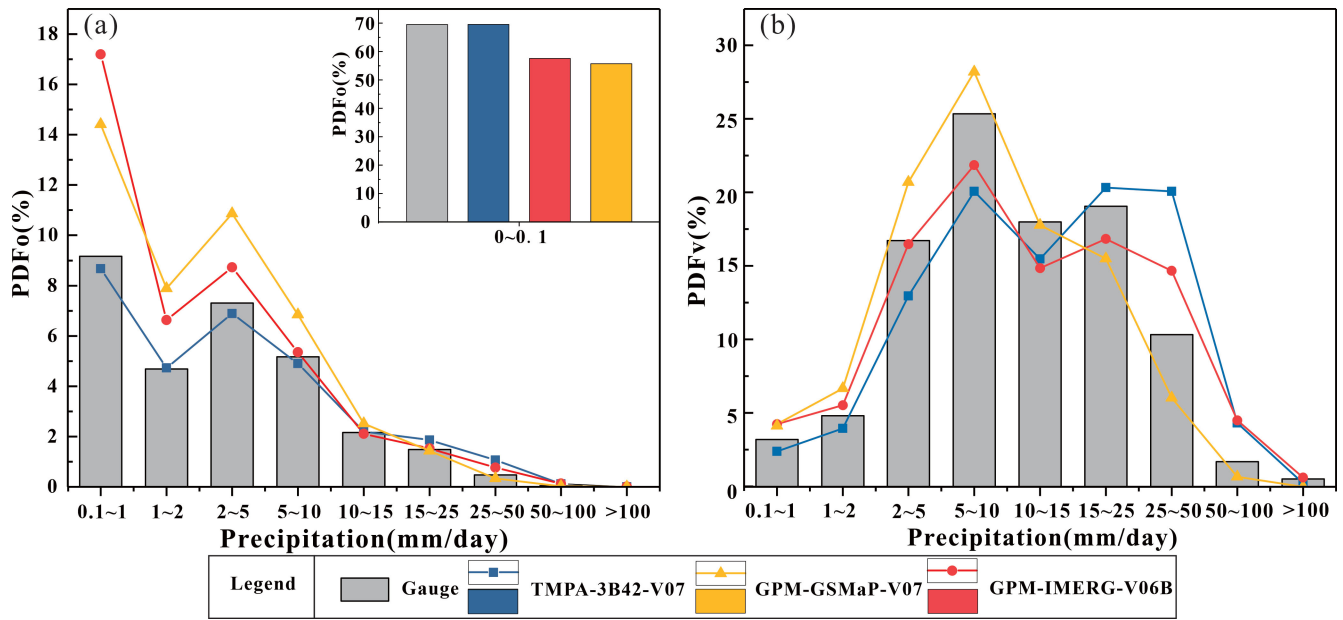


Fig. 3. PDFo (a) and by volume (PDFv) (b) for rain-gauges, IMERG, GSMaP, and TMPA with different intensities at daily scale for the 5-year study period (January 2015–December 2019).

against the rain-gauges observations during 2015 to 2019 at each gauge station over the TP.

In general, TMPA-3B42-V07 and IMERG-V06B products showed limited capability in estimating daily rainfall within the TP, with average CC values of about 0.24 and 0.31, respectively. GSMaP-V07 agreed better with the rain-gauge data over the TP, with an average CC value of 0.47. The CC values of all the satellite products were lower than 0.2 in the arid region like Qaidam and Qiangtang Basin. Overall, TMPA-3B42-V07, IMERG-V06B, and GSMaP-V07 products showed an overestimation of nearly 35.85%, 33.94%, and 20.34%, respectively at the daily scale. However, several negative RB values for these satellite rainfall estimates were detected in the Qaidam Basin. As for RMSE and MAE, the satellite products decreased gradually from the southeast to northwest across the TP. The average values of MAE were 2.12, 1.91, and 1.54 mm while that of RMSE were 0.14, 0.13, and 0.1 mm, respectively for TMPA-3B42-V07, IMERG-V06B, and GSMaP-V07.

Concerning POD, GSMaP showed much better performance than TMPA-3B42-V07 and IMERG-V06B in most regions except in Qaidam and Qiangtang Basin, while IMERG-V06B was better than TMPA-3B42-V07. Meanwhile, CSI and ETS had very similar distribution patterns with POD. The mean POD values were 0.5, 0.69, and 0.81, whereas the mean FAR values were 0.47, 0.47, and 0.40 for TMPA-3B42-V07, IMERG-V06B, and GSMaP-V07, respectively. Moreover, the mean CSI values were 0.35, 0.43, and 0.53 while that of ETS were 0.18, 0.23, and 0.35 for TMPA-3B42-V07, IMERG-V06B, and GSMaP-V07, respectively. This demonstrated that GSMaP had better detection accuracy and all the satellite rainfall products had about half of the FAR.

Hence, comparing the satellite rainfall products, GSMaP-V07 demonstrated better estimation over the whole TP with higher CC, POD, CSI, ETS as well as lower FAR, RBias, MAE, and

RMSE. IMERG-V06B had very similar distribution patterns with TMPA-3B42-V07, but IMERG showed better quality than TMPA within the TP.

Fig. 5 displays the spatial distributions of selected evaluation metrics (CC, RBias, MAE, RMSE) for monthly satellite precipitation against rain-gauge observations from 2015 to 2019 at each gauge station over the TP. Overall, TMPA-3B42-V07, IMERG-V06B and GSMaP-V07 showed an overestimation at a monthly scale, though the monthly precipitation performances were satisfied over the TP, having average CC values of 0.893, 0.916, and 0.924 respectively. As for the spatial distributions of selected metrics, monthly scale metrics showed similar distribution patterns with the daily scale metrics. The evaluation metrics of the satellite rainfall products at the monthly scale demonstrated that GSMaP-V07 had better estimation over the whole TP, with higher CC and lower RBias, MAE, and RMSE values. The performance of IMERG-V06B was close to GSMaP-V07, and showed better quality than TMPA over the TP.

Fig. 6 shows the box plot of rain-gauge station-based statistics for TMPA-3B42-V07, IMERG-V06B, and GSMaP-V07 at a daily and monthly scales over the TP. For each box, the central mark represents the median while the edges of the box are the 25th and 75th percentiles. On a daily scale, GSMaP-V07 performed better than TMPA-3B42-V07 and IMERG-V06B with higher CC and lower RBias, MAE, and RMSE values. Meanwhile, there were fewer outliers in GSMaP-V07 than TMPA-3B42-V07 and IMERG-V06B. For contingency statistics, IMERG-V06B and GSMaP-V07 had much higher POD, CSI, ETS, and lower FAR values than TMPA-3B42-V07, whereas GSMaP-V07 showed better performance.

On a monthly scale, the satellite products showed similar performances with each other. However, GSMaP-V07 revealed a more reliable performance than TMPA-3B42-V07 and IMERG-V06B using CC, RBias, MAE, and RMSE values. Fig. 7

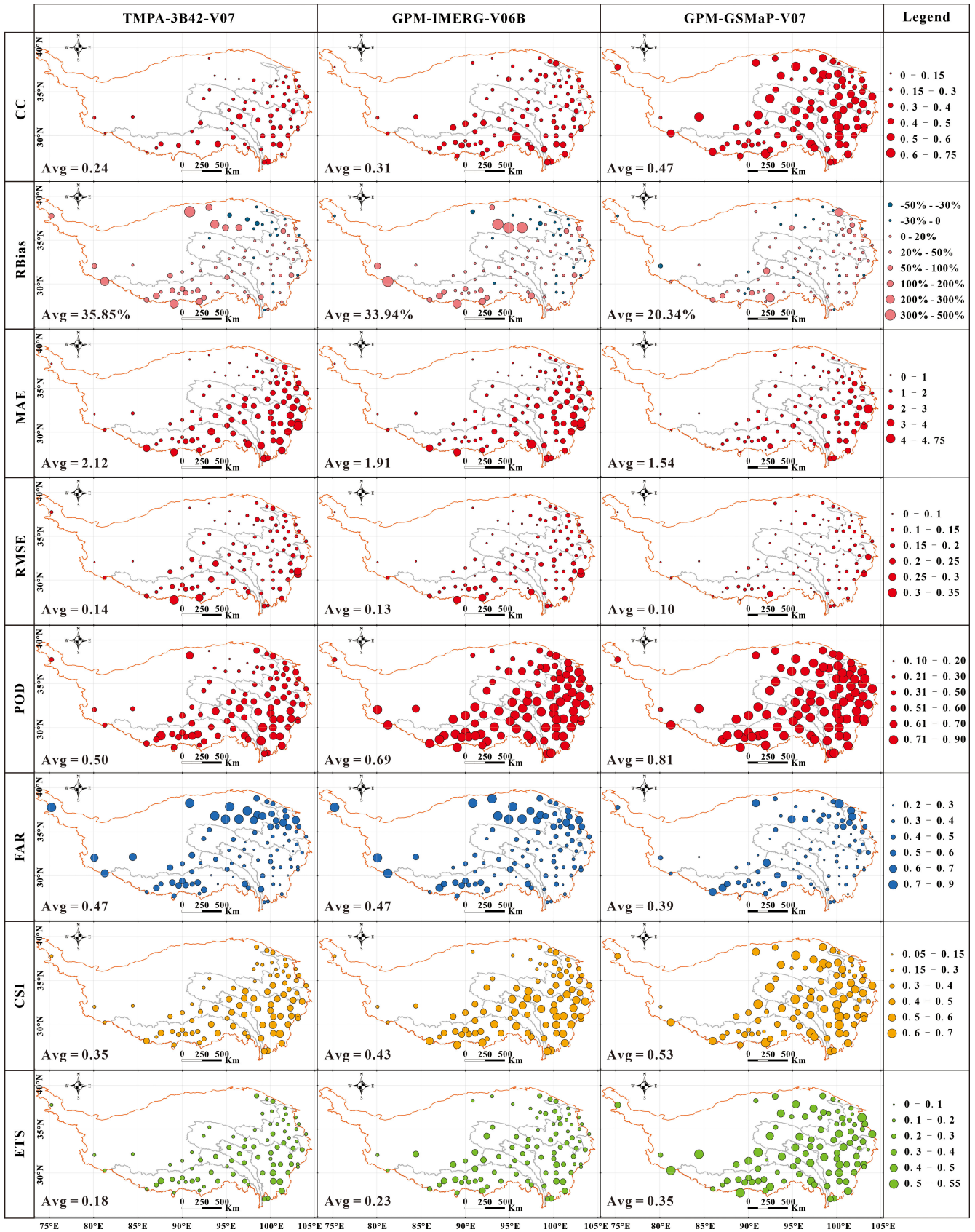


Fig. 4. Maps of CC, RBias, MAE, RMSE, and POD, FAR, CSI, ETS for the TP of IMERG, GSMaP, and TMPA 3B42 against rain-gauges data at daily scale (January 2015 to December 2019) over the TP.

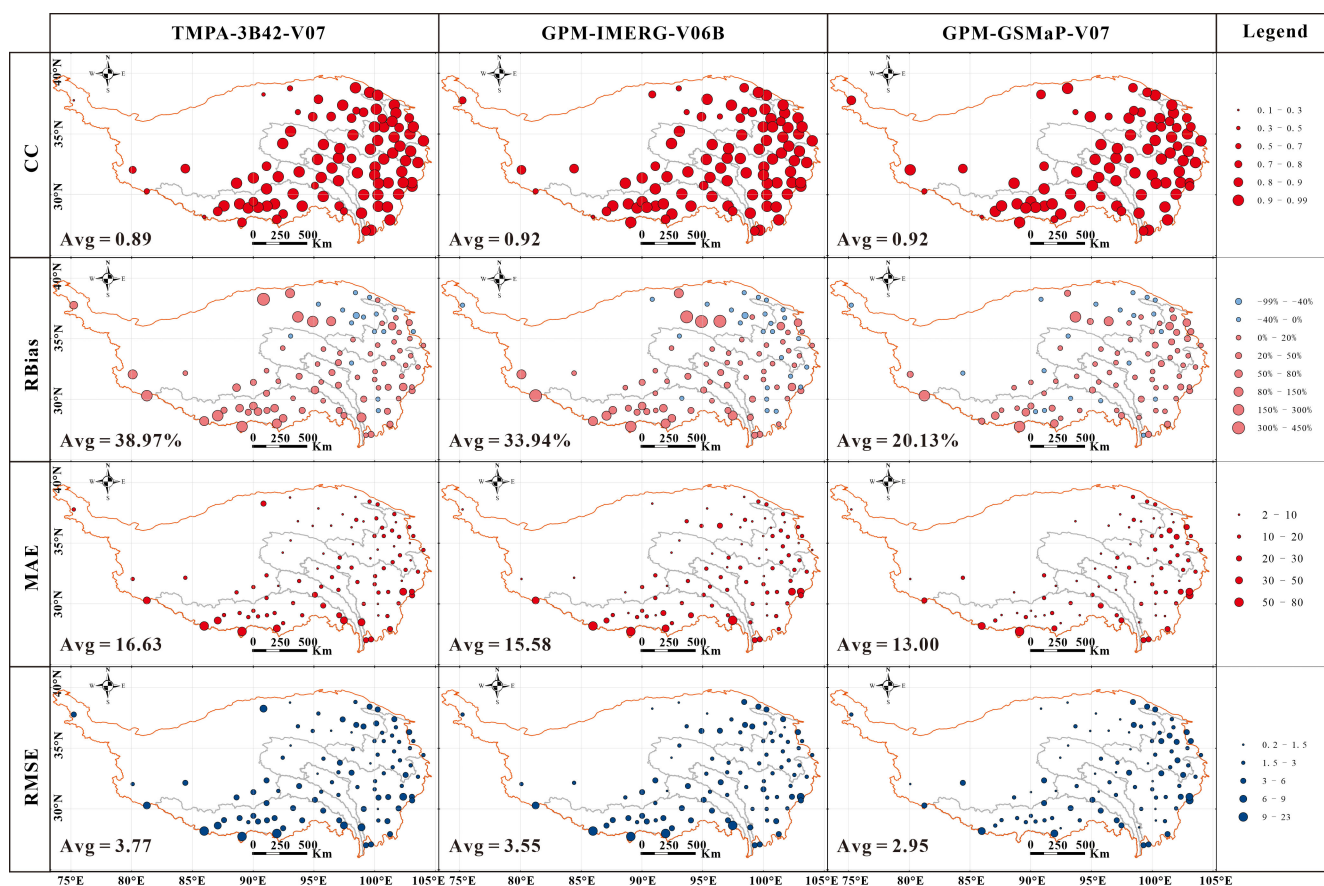


Fig. 5. Maps of CC; RBias; MAE; RMSE against rain-gauges data at monthly scale (January 2015 to December 2019) over the TP.

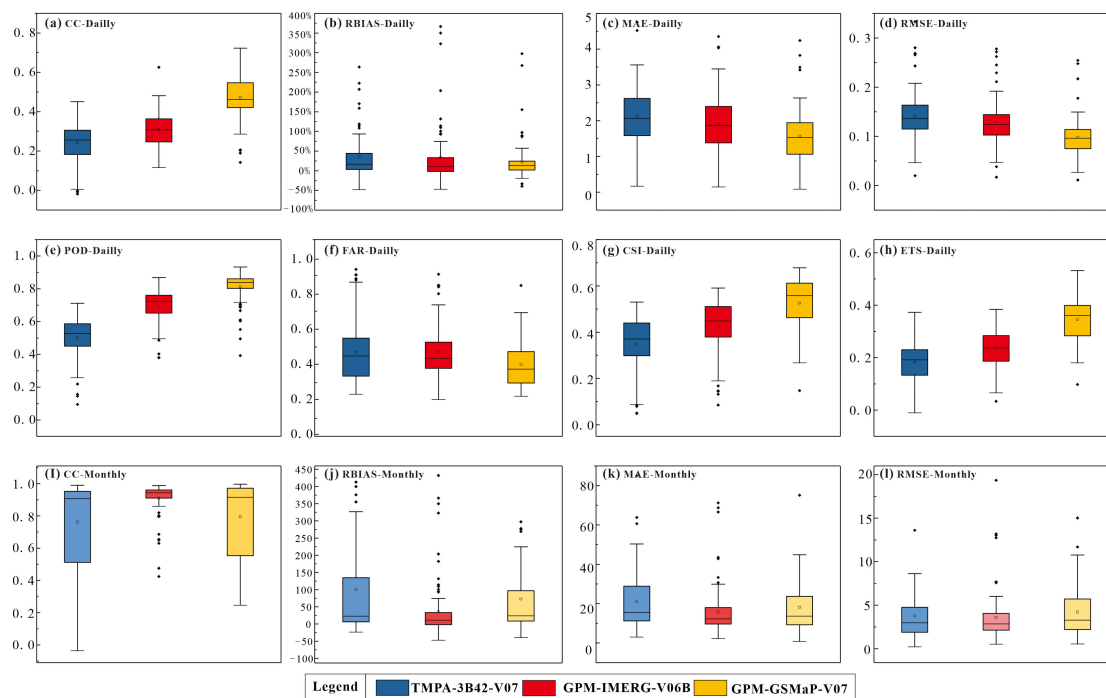


Fig. 6. Box plot of grid-based metrics: CC, RBias, MAE, RMSE, POD, FAR, CSI, and ETS at daily scale and CC, RBias, MAE, and RMSE at monthly scale for the 5-year study period (January 2015–December 2019).

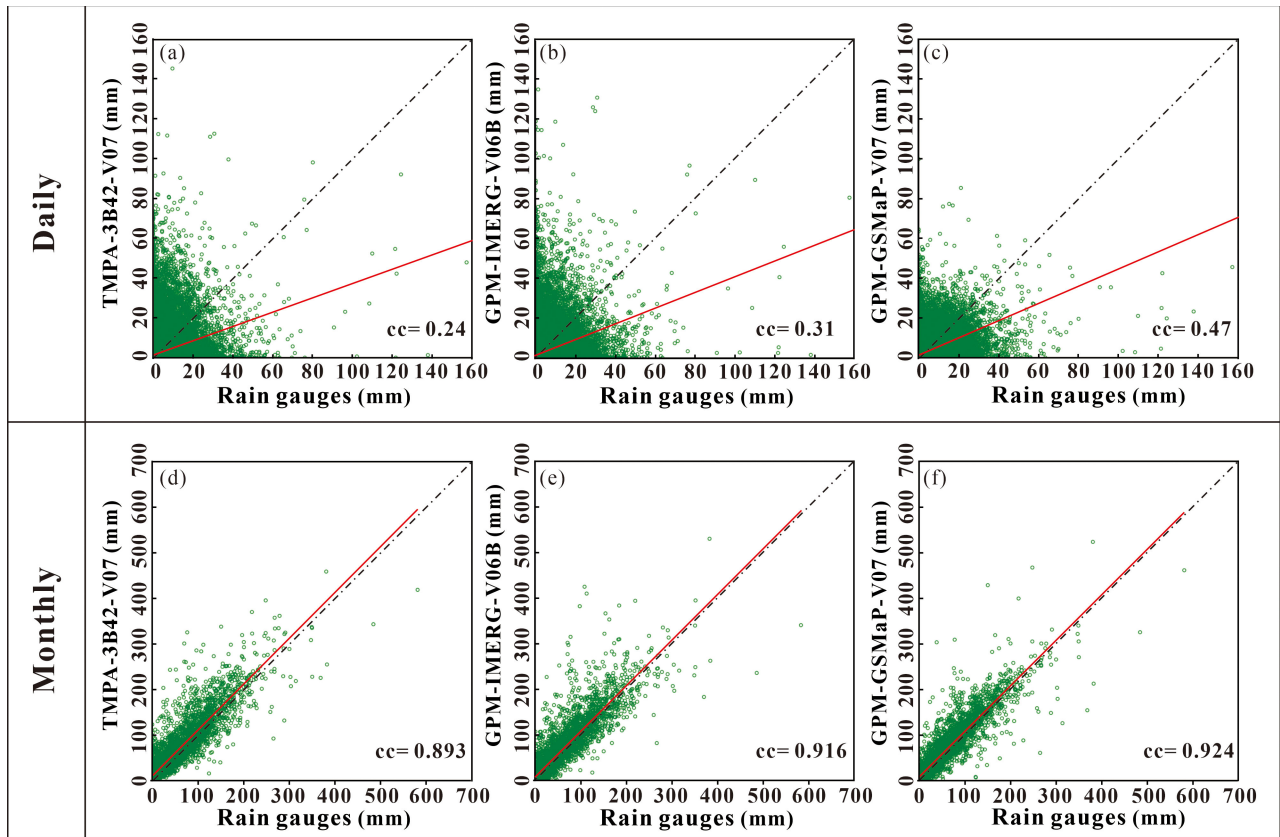


Fig. 7. Scatterplots for precipitation products versus rain-gauge measurements from 2015 to 2019 over the TP: (a–c) daily and (d–f) monthly, respectively.

shows the scatterplots of TMPA-3B42-V07, IMERG-V06B, and GSMaP-V07 versus rain-gauge measurements at daily and monthly scales from 2015 to 2019 over the TP. From this figure, all the satellite precipitation products showed lower consistency at a daily scale, with small CC values (0.24 for TMPA-3B42-V7, 0.31 for IMERG-V07, 0.47 for GSMaP-V06). The CC values significantly increased from daily scale to monthly scale (0.893, 0.916, 0.924), meaning that the performances of TMPA-3B42-V07, IMERG-V06B, and GSMaP-V07 significantly improved at monthly scale.

3) Performance Analysis by Rain Intensity: Detailed statistics of the error characteristics for TMPA-3B42-V07, IMERG-V06B, and GSMaP-V07 products regarding different rain intensities are provided in Table IV. Besides, Taylor diagrams (Fig. 8) are plotted to graphically summarize how well the three different precipitation datasets estimates. The rain-gauge observation is marked with a red dot, and the closer the marker of satellite precipitation estimates is to the rain-gauge observation, the better performance the product has.

For all rainfall events, more than 85% of the precipitation is light rain (0.1~10 mm/d), and rainfall volume of light rain accounted for about 50%. Satellite precipitation products showed an overestimation of light rain, and the RBias were 18.20%, 21.73%, and 25.54% for TMPA-3B42-V07, IMERG-V06B, and GSMaP-V07, respectively. GSMaP had higher CC (about 0.26), POD (0.83) and lower MAE (2.89), RMSE (0.02), FAR (0.17)

showing a relatively better performance in detecting light rain events.

As for moderate rain, heavy rain, rainstorm, and large rainstorm (10~25, 25~50, 50~100, and >100 mm/d), the satellite products had an obvious underestimation, with RBias values less than -50%. The POD and FAR has significant improvement in moderate rains, heavy rains, rainstorms, and large rainstorms detection than light rain, but the errors were increasing significantly. It can be seen that GSMaP-V07 has relatively better performance in detecting moderate rain (10~25 mm/d) with higher CC (0.13), POD (0.96), and lower MAE (8.82), RMSE (0.15), FAR (0.04) values.

Generally, GSMaP-V07 showed a better representation of precipitation than TMPA-3B42-V07 and IMERG-V06B, having a higher correlation and lower standard deviation ratio. Comparing the Taylor diagram as well as overall statistics during the study period, it was confirmed that GSMaP-V07 showed better results than TRMM-3B42-V7 and IMERG-V06B in detecting light and moderate rain, while all satellite products had limited capacity in detecting heavy rain, rainstorms, and large rainstorms.

4) Performance Analysis of Elevation Impact: Variations in evaluation metrics with increasing elevation are investigated and reported in Table V. The Taylor diagram (Fig. 9) was plotted to determine the impact of elevation on the accuracy of the satellite precipitation products. GSMaP-V07 demonstrated better

TABLE IV
SUMMARY OF EVALUATION METRICS FOR TMPA-3B42-V07, IMERG-V06B, AND GSMaP-V07 CALCULATED WITH ALL RAIN-GAUGES AT DAILY SCALES FOR DIFFERENT RAINFALL INTENSITIES FROM 2015 TO 2019

Rain intensity	Product	CC	RBias	MAE	RMSE	POD	FAR	CSI	ETS
Light Rain	TMPA-3B42-V07	0.14	18.20%	3.98	0.04	0.51	0.49	0.51	0.51
	IMERG-V06B	0.16	21.73%	3.60	0.03	0.70	0.30	0.70	0.70
	GSMaP-V07	0.26	25.54%	2.89	0.02	0.83	0.17	0.83	0.83
Moderate Rain	TMPA-3B42-V07	0.08	-55.29%	11.73	0.19	0.72	0.28	0.72	0.72
	IMERG-V06B	0.08	-52.35%	10.93	0.18	0.88	0.12	0.88	0.88
	GSMaP-V07	0.13	-46.49%	8.82	0.15	0.96	0.04	0.96	0.96
Heavy Rain	TMPA-3B42-V07	0.07	-70.75%	24.84	1.05	0.77	0.23	0.77	0.77
	IMERG-V06B	0.08	-65.99%	23.95	1.02	0.90	0.10	0.90	0.90
	GSMaP-V07	0.06	-65.55%	21.62	0.92	0.97	0.03	0.97	0.97
Rainstorm	TMPA-3B42-V07	0.36	-74.73%	46.46	6.46	0.84	0.16	0.84	0.84
	IMERG-V06B	0.40	-71.10%	44.39	6.19	0.91	0.09	0.91	0.91
	GSMaP-V07	0.14	-69.63%	42.33	5.96	0.95	0.05	0.95	0.95
Large Rainstorm	TMPA-3B42-V07	0.15	-71.31%	87.63	30.99	0.89	0.11	0.89	0.88
	IMERG-V06B	0.28	-72.74%	89.38	31.66	1.00	0.00	1.00	1.00
	GSMaP-V07	0.72	-83.11%	102.12	34.26	1.00	0.00	1.00	1.00

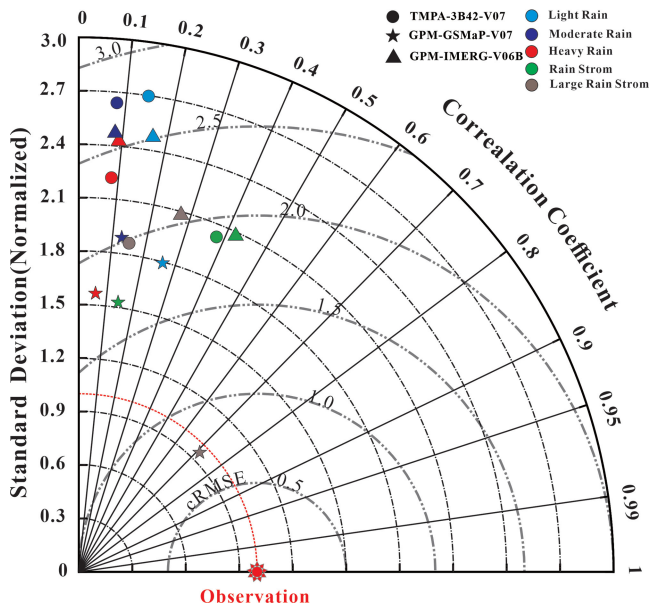


Fig. 8. Taylor diagrams consisting of CC and ratio of standard deviation for daily estimates for TMPA-3B42-V07, IMERG-V06B, and GSMaP-V07 over the TP for different rain intensities; light rain(0.1~10 mm/d); moderate rain (10~25 mm/d); heavy rain (25~50 mm/d); rainstorm (50~100 mm/d); large rainstorm (>100 mm/d).

capability by adequately capturing daily rainfall events compared to TMPA-3B42-V07 and IMERG-V06B, having higher CC and POD and lower MAE, RMSE, and FAR values at

different elevations. Besides, all satellite precipitation products overestimated precipitation at different elevations, which was obvious at the elevations over 4000 m.

In general, these evaluation metrics with the varying topographic elevation are not obvious, mainly because the weather stations used to evaluate the impact of elevation are not representative. As is well known, the TP and adjacent mountain ranges include Himalayas, Karakoram, Pamir, Kunlun, and Qilian mountains. From Fig. 1, we can see that the weather stations are sparsely distributed over the TP. To better understand the relationship between satellite precipitation products accuracy and elevation, the weather stations on northern slope of the Himalayas (mainly distributed in the southern TP region and Source Region of the Yarlung zangbo (SRYLZB) River basin) where the stations are relatively abundant are used in evaluation. The weather stations used to evaluate the elevation effect on the performance of the satellite precipitation products are listed in the Appendix (Table VIII.) There are 5, 8, and 7 stations in the 2300~3000, 3500~4000, and 4000~4500m elevation intervals, respectively, but there is no station in the 3000~3500m interval. The POD, FAR, CC, RBias, MAE, and RMSE in different elevation intervals on northern slope of the Himalayas are showed in Fig. 10.

The POD in 2300~3000, 3500~4000, 4000~4500 m elevation intervals are comparative similar for three products, but the FAR are higher in 3500~4000 and 4000~4500 m elevation intervals. Furthermore, CC values tends to be lower in 3500~4000 and 4000~4500 m elevation intervals than 2300~3000 m elevation interval. It does show that the satellite products greatly

TABLE V
SUMMARY OF EVALUATION METRICS FOR TMPA-3B42-V07, IMERG-V06B, AND GSMaP-V07 CALCULATED WITH ALL RAIN-GAUGES AT DAILY SCALES FOR DIFFERENT ELEVATION FROM 2015 TO 2019

Elevation	Product	CC	RBias	MAE	RMSE	POD	FAR	CSI	ETS
<2500	TMPA-3B42-V07	0.29	14.56%	2.53	0.05	0.50	0.46	0.35	0.18
	IMERG-V06B	0.36	18.74%	2.37	0.05	0.70	0.48	0.42	0.22
	GSMaP-V07	0.39	28.20%	2.23	0.04	0.84	0.46	0.49	0.28
2500~3000	TMPA-3B42-V07	0.31	18.30%	2.04	0.04	0.49	0.50	0.33	0.18
	IMERG-V06B	0.37	23.03%	1.89	0.03	0.68	0.52	0.39	0.21
	GSMaP-V07	0.48	12.17%	1.52	0.03	0.82	0.42	0.52	0.36
3000~3500	TMPA-3B42-V07	0.28	8.99%	2.38	0.04	0.55	0.42	0.39	0.20
	IMERG-V06B	0.32	4.73%	2.13	0.03	0.70	0.43	0.46	0.24
	GSMaP-V07	0.51	8.88%	1.73	0.03	0.83	0.36	0.57	0.37
3500~4000	TMPA-3B42-V07	0.30	13.38%	2.28	0.04	0.58	0.36	0.43	0.24
	IMERG-V06B	0.32	12.45%	2.09	0.04	0.76	0.42	0.49	0.25
	GSMaP-V07	0.50	15.27%	1.68	0.03	0.85	0.33	0.60	0.39
4000~4500	TMPA-3B42-V07	0.27	30.06%	2.15	0.03	0.54	0.38	0.40	0.23
	IMERG-V06B	0.30	25.61%	1.92	0.03	0.73	0.41	0.49	0.28
	GSMaP-V07	0.50	17.56%	1.48	0.02	0.83	0.34	0.58	0.40
>4500	TMPA-3B42-V07	0.28	33.37%	1.83	0.04	0.50	0.48	0.34	0.19
	IMERG-V06B	0.34	28.15%	1.60	0.03	0.69	0.48	0.42	0.25
	GSMaP-V07	0.50	8.95%	1.19	0.02	0.80	0.39	0.53	0.38

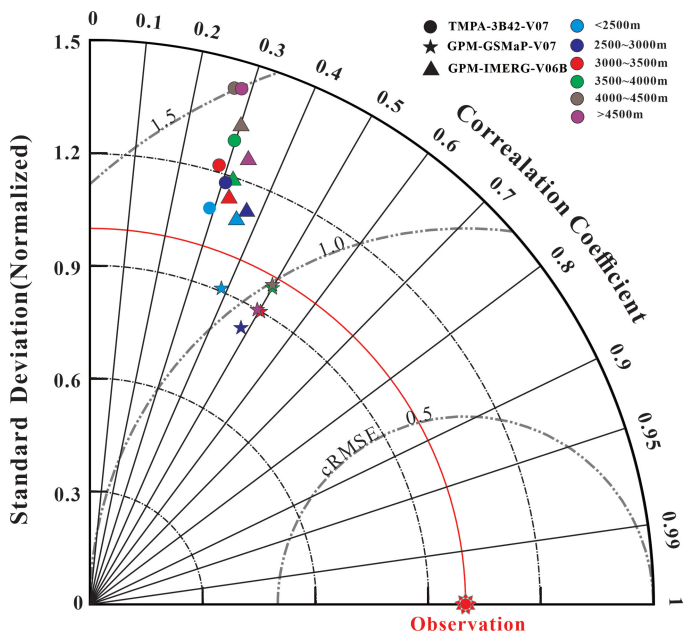


Fig. 9. Taylor diagrams consisting of CC and ratio of standard deviation for daily estimates for TMPA-3B42-V07, IMERG-V06B, and GSMaP-V07 over the TP at different elevations.

overestimated the precipitation at high-elevation (>4000 m) regions, which had RBias values larger than 50% for all three products. Therefore, all TMPA-3B42-V07, IMERG-V06B, and GSMaP-V07 products have performed relatively better in lower elevation (<3000 m) regions, with higher CC values and lower RBias and FAR values.

5) *Performance Analysis at the Basin Scale:* To facilitate researchers to use satellite precipitation data in hydrological simulation and flood forecasting at the basin scale, we considered the basin scale analysis to evaluate performances of the satellite products over the subbasins within the TP. Detailed statistics of the error characteristics for TMPA-3B42-V07, IMERG-V06B, and GSMaP-V07 products over seven subregions are provided in Table VI. Also, Taylor diagrams (Fig. 11) are plotted to graphically summarize how well the three different precipitation datasets estimates.

For the GSMaP-V07 daily scale, CC values (0.45~0.53) tends to be higher than TMPA-3B42-V07 (0.11~0.32) and IMERG-V06B (0.25~0.4), and also tends to be higher at the Source Region of the Yangtze Rivers (SRYZR), Source Region of the Lancang River (SRLCR), and Source Region of the Nujiang River (SRNR) basins. It is worth noting that the satellite products greatly overestimated the precipitation in SRYLZBR,

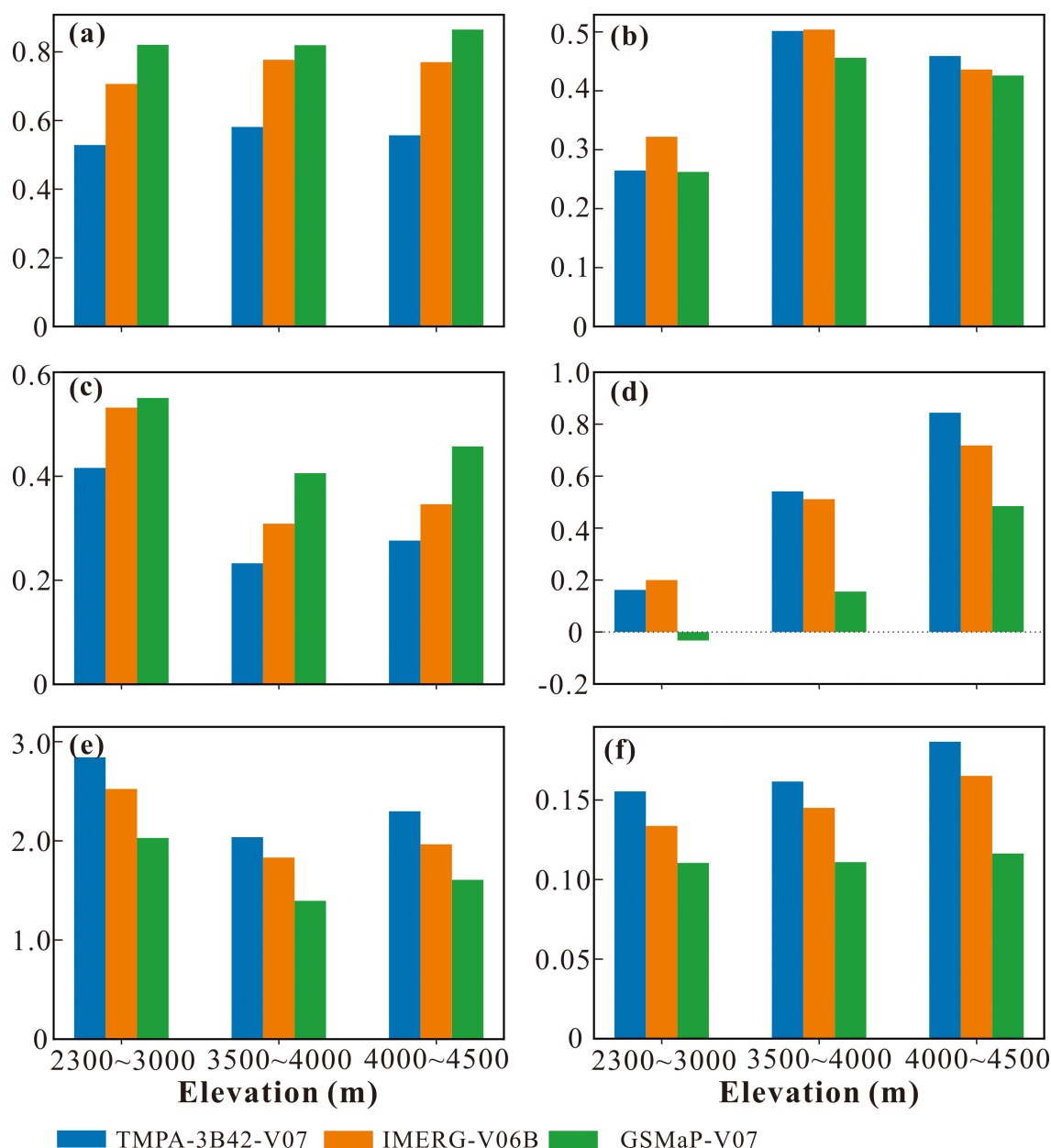


Fig. 10. (a) POD. (b) FAR. (c) CC. (d) RBias. (e) MAE. (f) RMSE from TMPA-3B42-V07, IMERG-V06B, and GSMaP-V07 over different elevation ranges on northern slope of the Himalayas.

which had RBias values of about 49.46%, 54.02%, 19.79% for TMPA-3B42-V07, IMERG-V06B, and GSMaP-V07, respectively. High overestimation was found in QTB using TMPA-3B42-V07 and IMERG-V06B (50.17% and 50.47%) and in QDMB utilizing IMERG-V06B (49.47%). GSMaP had a much better estimation in QTB and QDMB (RBias of 16.14% and 18.26%).

The spatial patterns of POD, FAR, CSI, ETS values at the subbasin scale for both products showed that GSMaP-V07 performed better than TMPA-3B42-V07 and IMERG-V06B in all basins. Detection performance was much better in SRYZR, SRLCR, SRNR, and SRYLZBR basins located in the semi-humid areas than in SRYR, QTB, QDMB basins

located in arid and semi-arid areas. Therefore, satellite precipitation products performed better in basins located within the semi-humid areas than arid and semi-arid areas over the TP.

Despite all this, when examining all the eight indices within the seven subbasins over the TP, it was clear that the satellite precipitation products performed better in SRYR, SRYZR, SRLCR, and SRNR basins. GSMaP-V07 showed an apparent advantage over TMPA-3B42-V07 and IMERG-V06B, while TMPA-3B42-V07 and IMERG-V06B had comparable performances with each other, though IMERG-V06B was slightly better than TMPA-3B42-V07. In the arid climate regions, GSMaP had better performance than other products.

TABLE VI
SUMMARY OF EVALUATION METRICS FOR TMPA-3B42-V07, IMERG-V06B, AND GSMaP-V07 CALCULATED WITH ALL RAIN GAUGES AT DAILY SCALES FOR SEVEN SUBBASINS FROM 2015 TO 2019

Basin	Product	CC	RBias	MAE	RMSE	POD	FAR	CSI	ETS
SRYR	TMPA-3B42-V07	0.25	5.56%	2.24	0.03	0.49	0.43	0.36	0.17
	IMERG-V06B	0.28	6.41%	2.07	0.03	0.69	0.47	0.43	0.20
	GSMaP-V07	0.45	18.61%	1.78	0.02	0.84	0.41	0.53	0.32
SRYZR	TMPA-3B42-V07	0.30	11.57%	2.69	0.03	0.56	0.34	0.43	0.23
	IMERG-V06B	0.34	6.14%	2.42	0.03	0.72	0.38	0.50	0.26
	GSMaP-V07	0.47	13.17%	2.03	0.02	0.84	0.32	0.61	0.39
SRLCR	TMPA-3B42-V07	0.32	23.36%	2.44	0.06	0.59	0.40	0.43	0.20
	IMERG-V06B	0.40	24.32%	2.19	0.06	0.73	0.39	0.50	0.26
	GSMaP-V07	0.50	9.58%	1.68	0.04	0.84	0.32	0.60	0.39
SRNR	TMPA-3B42-V07	0.26	32.56%	2.38	0.09	0.56	0.41	0.40	0.21
	IMERG-V06B	0.28	20.06%	2.03	0.08	0.76	0.46	0.46	0.22
	GSMaP-V07	0.52	14.41%	1.61	0.05	0.83	0.39	0.54	0.33
SRYLZBR	TMPA-3B42-V07	0.29	49.46%	2.34	0.04	0.56	0.44	0.39	0.22
	IMERG-V06B	0.38	54.02%	2.14	0.04	0.76	0.44	0.47	0.29
	GSMaP-V07	0.44	19.79%	1.66	0.03	0.84	0.41	0.53	0.34
QTB	TMPA-3B42-V07	0.25	50.17%	1.39	0.04	0.48	0.57	0.29	0.18
	IMERG-V06B	0.31	50.47%	1.23	0.04	0.72	0.55	0.38	0.25
	GSMaP-V07	0.47	16.14%	0.86	0.03	0.78	0.43	0.49	0.39
QDMB	TMPA-3B42-V07	0.11	16.23%	0.73	0.02	0.27	0.81	0.13	0.05
	IMERG-V06B	0.25	49.47%	0.75	0.02	0.56	0.75	0.21	0.12
	GSMaP-V07	0.53	18.26%	0.47	0.02	0.74	0.58	0.37	0.30

C. Hourly Scale Statistical Performances of Satellite Precipitation Estimates in One Grid Box

Hourly scale statistical performances were conducted for one grid box value of IMERG-V06B and GSMaP-V07 versus Thiessen polygon averaged precipitation over 15 rain-gauges from August 1, 2019 to September 30, 2019. The distribution of high-density networks of rain-gauges is shown in Fig. 11. Precipitation from the 15 rain-gauges varied from 120 mm~173 mm, with uneven spatial distributions (Fig. 12). Moreover, precipitation was higher in higher altitude in the grid box, which means that satellite products cannot depict the fine distribution of precipitation in a complex mountain area.

The two-month accumulated precipitation from the grid box calculated by the arithmetic average and Thiessen polygon method are 138 and 147 mm, respectively. The precipitation values of IMERG-V06B and GSMaP-V07 were 211 and 218 mm, which is about 43.54% and 48.3% higher than Thiessen polygon's average precipitation. In the grid-based hourly scale evaluation, IMERG-V06B and GSMaP-V07 products showed an

obvious overestimation of about 43.47% and 48.24%, respectively. IMERG-V06B with a CC and POD values of 0.03 and 0.26 had poor consistency with rain-gauge observations while GSMaP-V07 having CC and POD values of 0.42 and 0.59 had a better agreement with rain-gauge data.

The precipitation processes in one grid-box are shown in Fig. 13. We observed that there were relatively obvious random errors in the IMERG-V06B and GSMaP-V07 products. Consequently, the random errors resulted in severe overestimation in the satellite precipitation estimation, which was more evident in IMERG-V06B product. GSMaP-V07 had a better consistency with rain-gauge observations while IMERG-V06B had an obvious overestimation of nearly 100%~500% for some light rain processes (<5 mm/d).

Fig. 14 shows the scatterplots between satellite precipitation products and Thiessen polygon averaged precipitation. The evaluation metrics of IMERG-V06B and GSMaP-V07 versus Thiessen averaged precipitation at hourly scale are provided in Table VII. In one grid-based hourly scale evaluation,

TABLE VII
SUMMARY OF EVALUATION METRICS FOR ONE GRID BOX VALUE OF IMERG-V06B AND GSMaP-V07 VERSUS THIESSEN POLYGON AVERAGED PRECIPITATION AT HOURLY SCALES FROM AUGUST 1, 2019 TO SEPTEMBER 30, 2019

Station	Satellite	POD	FAR	CSI	ETS	CC	RBias	MAE	RMSE
Thiessen	IMERG-V06B	0.26	0.75	0.14	0.07	0.03	43.47%	0.23	0.02
averaged	GSMaP-V07	0.59	0.64	0.29	0.20	0.43	48.24%	0.16	0.01

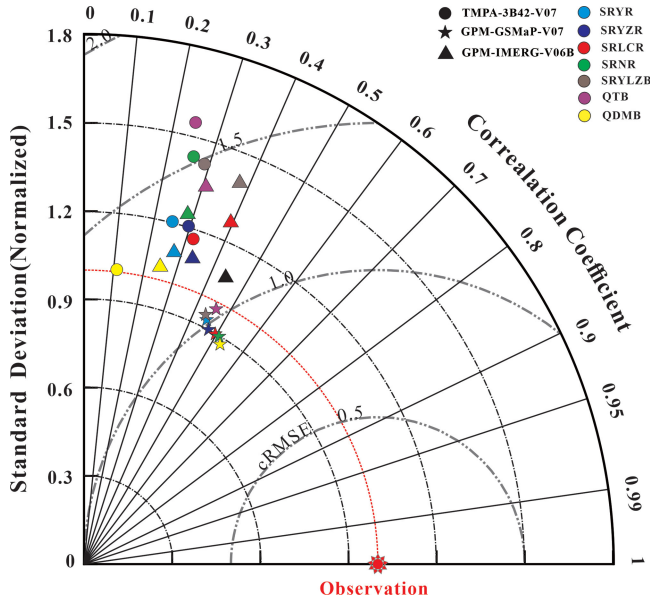


Fig. 11. Taylor diagram showing CC, standard deviation (normalized), and RMSE for daily precipitation estimates from TMPA-3B42-V07, IMERG-V06B, and GSMaP-V07 over seven sub-regions.

IMERG-V06B and GSMaP-V07 products showed an obvious overestimation of about 43.47% and 48.24%, respectively. Moreover, IMERG-V06B had poor consistency with rain-gauge observations, with CC of 0.03 and POD of 0.26. GSMaP-V07 was in better agreement with rain-gauge data, with the CC value of 0.43 and POD value of 0.59. Accordingly, GSMaP-V07 had better detection accuracy at an hourly scale, meaning that hourly precipitation detection was very difficult for satellite in a complex mountain area.

IV. DISCUSSION

GPM-IMERG-V07 and GPM-GSMaP-V06 products are estimated from passive microwave (PMW) sensors, geo-infrared data source integrating the morphing technique (i.e., morph), and DPR. Five PMW instruments contribute to IMERG-V07 and GSMaP-V06, which includes GMI, AMSR2, AMSU-A/MHS, SSMIS, and TMI [38], [42]. It is noteworthy that the constitution of the PMW sources changes with time, and PMW sensors including imagers (GMI, AMSR2, SSMIS, and TMI) and sounders (AMSU-A/MHS). In the GPM-GSMaP system, over 50% of precipitation estimates are derived from the geo-IR morphing technique (i.e., morph), and about 45% of precipitation estimates are derived from PMW sensors [42]. In the GPM-IMERG system, over 65% of precipitation estimates are derived from

geo-IR morphing technique (i.e., morph) while nearly 30% of precipitation estimates are derived from PMW sensors [38]. This explained why GPM-GSMaP-V06 was superior to GPM-IMERG-V07.

The GPM combined instrument (GMI) sensor can capture light precipitation better than the TRMM combined instrument (TMI) [31], but GMI showed a noticeable overestimation of light and medium rainfall. SSMIS, AMSU-A/MHS and morph showed remarkable underestimation of heavy rainfall while TMI exhibited slight underestimation for the medium and heavy rainfall events. These are the main sources of overestimation of light rainfall and underestimation of heavy rainfall for all the three multisatellite products.

According to the evaluation metrics of the two GPM-era satellite precipitation products, the performances of GPM-GSMaP-V07 proved to be much better than GPM-IMERG-V06B over the TP. Microwave imager/sounder, IR Imager, and precipitation radar were the same for merging IMERG-V06B and GSMaP-V07 products [38], [42]. The better performances shown by GPM-GSMaP-V07 indicated that the GSMaP algorithm was better than the IMERG algorithm. Specifically, the GSMaP-V07 algorithm improved in the microwave imager algorithm based on the AMSR2 precipitation standard algorithm (including new land algorithm, new coast detection scheme, etc.), and made the development of microwave sounder algorithm overland [39].

The capability of IMERG-V06B and GSMaP-V07 in detecting rain and no-rain event in complex mountain areas could be acceptable, but it was found that all satellite products significantly overestimated the rain-gauge precipitation at daily and monthly scales. This was mainly because the satellite precipitation estimates usually overestimate light rain and were usually greater than zero when the gauges show no rain. Fig. 3 showed that no rain events and light precipitation events (0.1~10 mm/d) accounted for about 60% and 25%, respectively.

A few extremely high positive or negative relative biases (i.e., >100% and <-40%) and high FAR were detected in the QDMB basin in the northern part of the TP (Fig. 4). The QDMB basin has the arid plateau continental climate with the mean annual precipitation 170 mm and the precipitation has larger relative variability. High relative biases and FAR was mainly because the satellite precipitation estimation usually greater than zero when the gauges show no rain. The high positive biases (>100%) were detected in SRYLZBR (the southern TP). The positive biases in SRYLZBR may be due to the frequent orographic-convective warm cloud processes over the southern TP. The orographic-convective precipitation might not produce much ice phase particles aloft [43]–[45], therefore, more water particles in the clouds might cause the positive biases in

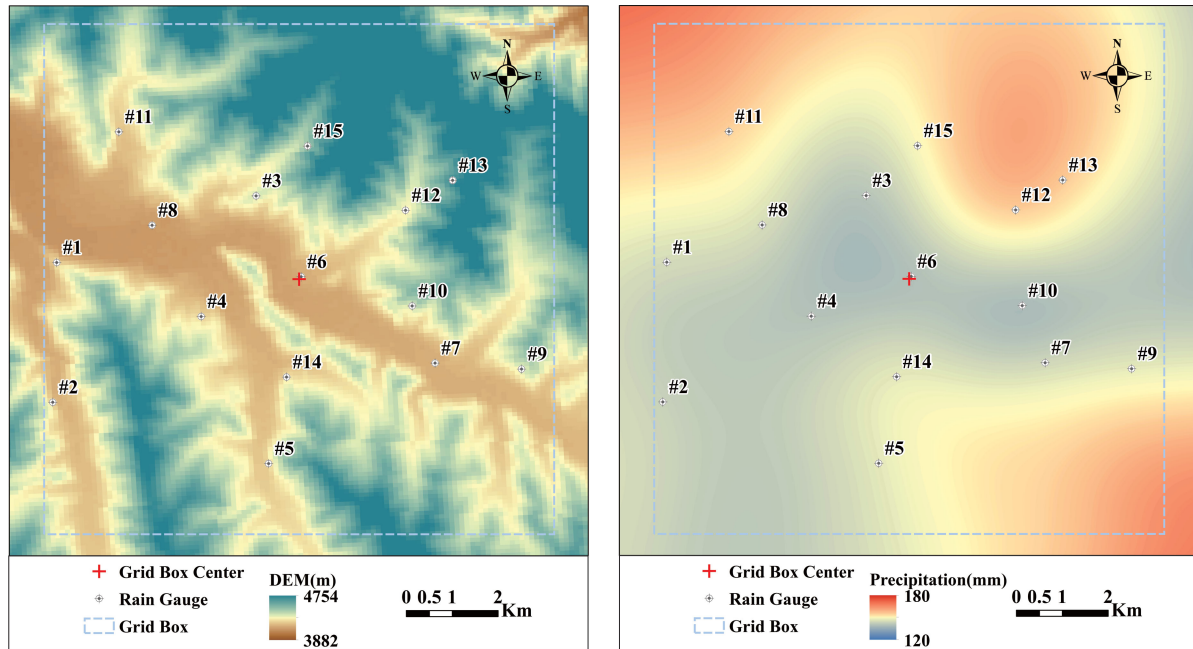


Fig. 12. Distribution of high-density network of rain gauges (15 tipping-bucket rain gauges installed in one GPM grid box) and DEM; Spatial distributions of two-month precipitation based on spline interpolation.

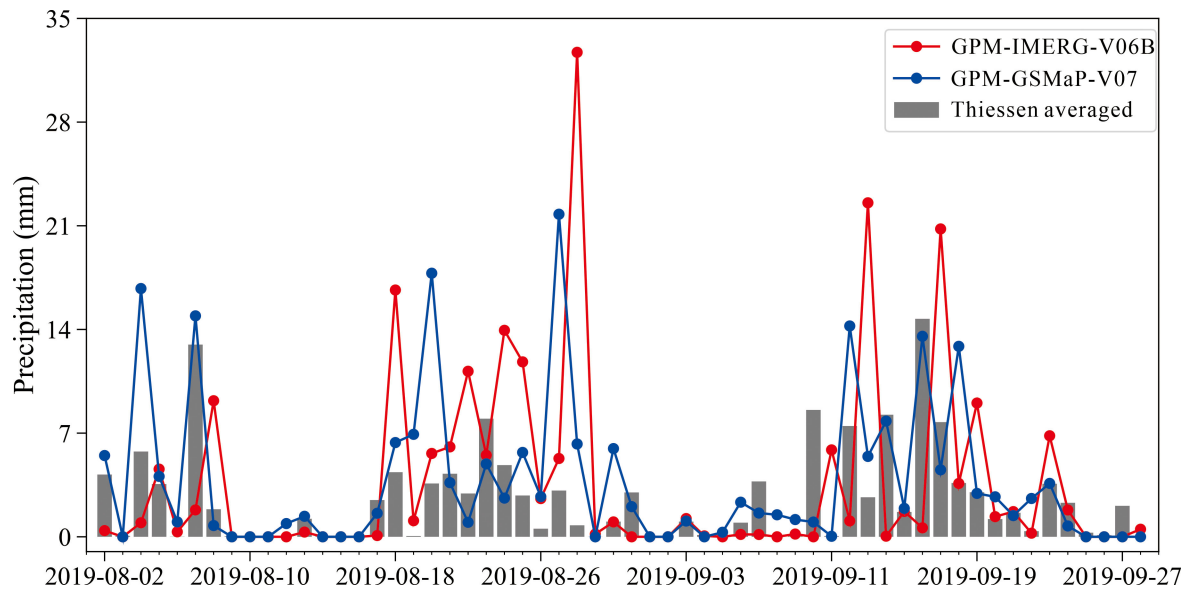


Fig. 13. Precipitation process comparison of the Thiessen averaged precipitation with IMERG-V06B and GSMaP-V07 at daily scale.

SRYLZBR. Orographic influences on the cloud microphysical processes and precipitation formation are complex, thus it can be concluded that satellite precipitation observing skills were greatly influenced by complex topography and huge mountains.

It can be seen from Figs. 6 and 7 that the performances of all the products were apparently getting better from daily to monthly scale. The CC values significantly improved when the time scale increased from hourly and daily to monthly scale for TMPA-3B42-V07 and GPM-IMERG-V06B, mainly because the GPCC monthly product was used for bias-correction of the TMPA and IMERG products [12], [46]. GPM-GSMaP-V07

showed the best performance on a daily scale, mostly because GSMaP products are corrected by CPC daily rain-gauges. The phenomenon was particularly obvious in the scatter plot (Fig. 7), that is, random errors were widespread in the scatter plot at the daily scale, but improved favorably at the monthly scale. Unlike systematic error, random errors are random means that they will diminish when averaging upscale [38]. It can be inferred that it is feasible and reliable using satellite products above a daily scale on a regional level.

Previous research [25], [47] has shown that TMPA-3B42 products have certain potentials for hydrological simulation

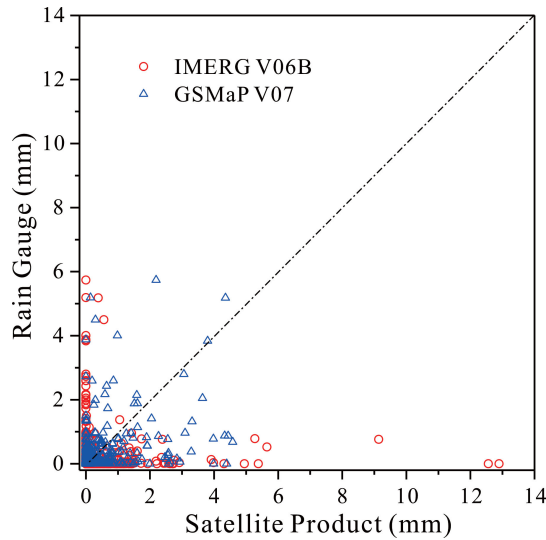


Fig. 14. Scatterplots of satellite precipitation products versus Thiessen polygon averaged precipitation over 15 rain-gauges from August 1, 2019 to September 30, 2019.

in the TP. GPM-era products improved based on the TRMM-era algorithm, so the IMERG and GSMaP datasets are both valuable for hydrological applications at basins in the TP where rain-gauges are sparsely distributed. Lu and Yong [34] investigated the performances in hydrological utility with calibrated/uncalibrated IMERG and GSMaP products in the SRYR. The research demonstrated that uncalibrated products showed unsatisfactory performance, whereas the calibrated GSMaP product showed a satisfactory hydrological application within the TP.

This study showed relatively better detecting ability for lower elevation (<3000 m) regions, but there are more than 50% overestimation at high-elevation (>4500 m) regions for all three satellite products. The limited detection skill at high-elevation (>4000 m) regions might be related to not only the snow-covered surfaces at high altitude but also the technological limitations for the solid precipitation [48], [49]. Strong scattering induced by snow-covered surfaces has an effect on microwave algorithms. In addition, complex precipitation patterns over the TP and the limited ground stations greatly restricted the evaluation of the elevation effect on the performance of the satellite precipitation products [50], [51].

V. SUMMARY AND CONCLUSION

This study evaluated the performances of two latest released two GPM-era satellite precipitation products and one TRMM-era product on a daily and monthly scale over the TP from January 2015 to December 2019. The performances of TMPA-3B42-V07, IMERG-V06B, and GSMaP-V07 at daily scale over the TP for different rain intensities, subbasins, and elevations were also evaluated. Furthermore, hourly scale statistical performances were conducted for one grid box value of IMERG-V06B and GSMaP-V07 versus 15 rain-gauges from August 1, 2019 to September 30, 2019. The main conclusion is summarized as follows.

- 1) The spatial distribution of mean annual precipitation showed a decreasing trend from southeast to northwest over the TP. All three multisatellite products significantly overestimated the rain-gauge precipitation at daily and monthly scales. The performances of the three products significantly improved from daily to monthly scale, with small CC values (0.24 for 3B42-V7, 0.31 for IMERG-V07, 0.47 for GSMaP-V06) at daily scale to higher CC values at monthly scale (0.893, 0.916, and 0.924).
- 2) In general, GPM-era satellite precipitation products (IMERG-V06B and GSMaP-V07) are considered a good replacement for TRMM-era standard products (TMPA-3B42-V07). TMPA-3B42-V07 and IMERG-V06B showed the same distribution pattern of performances, but IMERG-V06B showed better performance than TMPA-3B42-V07 with higher POD and CC values. At the daily scale, GSMaP-V07 outperforms TMPA-3B42-V07 and IMERG-V06B with higher CC and lower RBias, MAE, and RMSE values.
- 3) Satellite precipitation products showed an overestimation of light rain and underestimation of moderate rain, heavy rain, and rainstorm. More than 85% of precipitation over the TP is light rain (0.1~10 mm/d), and the volume accounts for about 50%. It can also be seen that all satellite products have limited capacity in detecting heavy rain, rainstorm, and large rainstorm.
- 4) The satellite products had performed relatively better in lower elevation (<3000 m) regions and greatly overestimated the precipitation at high-elevation (>4000 m) regions, which had RBias values larger than 50% for all three products.
- 5) Satellite precipitation products performed better in the SRYR, SRYZR, SRLCR, and SRNR basins. GSMaP-V07 has enormous potential for basin-scale hydrological applications. TMPA-3B42-V07 and IMERG-V06B had comparable quality as GSMaP in the SRYR, SRYZR, LCRB, and SRNR basins, but they had an obvious overall overestimation in the arid basins (QTB and QDMB) and humid region in southern TP (SRYLZBR).
- 6) In one grid-based hourly scale evaluation, satellite products had poor consistency with rain-gauges and showed an obvious overestimation in two months of the study period. GSMaP-V07 showed higher overestimation than IMERG-V06B at an hourly scale, but it has better consistency with rain-gauge observations.

The evaluation of the performances of the satellite products in this study could provide better understanding on the accuracy characteristics within the TP. One shortcoming of our study is the use of only one grid box for only two months at hourly scale evaluation. Based on these findings, we recommend that future multisatellite rainfall retrieval algorithms could focus on the improvement of overestimation of light rain and underestimation of moderate rain, heavy rain, and rainstorm over the TP. Furthermore, more available data from both high-density rain-gauges in complex mountainous regions and the latest released IMERG and GSMaP satellite products will be incorporated into the comprehensive statistical and hydrologic assessment in near future.

APPENDIX

TABLE VIII

WEATHER STATIONS USED TO EVALUATE THE ELEVATION EFFECT ON THE PERFORMANCE OF THE SATELLITE PRECIPITATION PRODUCTS ON NORTHERN SLOPE OF THE HIMALAYAS

No.	Code	Name	Province	Latitude	Longitude	Altitude
1	56434	Chayu	Xizang	28.65	97.47	2328
2	56459	Muli	Sichuan	27.93	101.27	2450
3	56548	Weixi	Yunnan	27.02	99.28	2459
4	56227	Bomi	Xizang	29.87	95.77	2736
5	56312	Linzhi	Xizang	29.07	94.03	2992
6	55598	Zedang	Xizang	29.25	91.77	3552
7	55591	Lasa	Xizang	29.07	91.13	3649
8	56331	Zuogong	Xizang	29.07	97.08	3780
9	55585	Nimu	Xizang	29.43	90.02	3809
10	55655	Nielaer	Xizang	28.18	85.97	3810
11	55578	Rikaze	Xizang	29.25	88.88	3836
12	55696	Longzi	Xizang	28.42	92.47	3860
13	55569	Lazi	Xizang	29.08	87.60	4000
14	55680	Jiangzi	Xizang	28.92	89.60	4040
15	55493	Dangxiong	Xizang	30.48	91.10	4200
16	55690	Cuona	Xizang	27.98	91.95	4280
17	55664	Dingri	Xizang	28.63	87.08	4300
18	55773	Pali	Xizang	27.73	89.08	4300
19	55681	Langkazi	Xizang	28.97	90.40	4432
20	56202	Jiali	Xizang	30.07	93.28	4489

ACKNOWLEDGMENT

This work was supported in part by the National key research and development project under Grants 2017YFC0403600, and 2016YFE0201900, in part by the National Natural Science Foundation of China under Grants 91847302, 51909130, in part by the National Natural Science Foundation of Technology Department of Qinghai Province under Grant 2019-ZJ-968Q, and in part by the State Key Laboratory of Hydro-science and

Engineering under Grant sklhse-2020-low01. The IMERG data were provided by the NASA Goddard Space Flight Center's Precipitation Processing System (PPS), which develops and computes IMERG as a contribution to GPM. The data are archived at NASA GES DISC. The GSMaP data obtained from the Earth Observation Research Center, Japan Aerospace Exploration Agency (EORC/JAXA). The authors would like to express their sincere thanks to the scientists in NASA and JAXA.

REFERENCES

- [1] W. W. Immerzeel, L. P. H. van Beek, and M. F. P. Bierkens, "Climate change will affect the Asian water towers," *Science*, vol. 328, no. 5984, pp. 1382–1385, 2010. [Online]. Available: www.jstor.org/stable/40656070
- [2] G. Wu *et al.*, "The influence of mechanical and thermal forcing by the Tibetan plateau on Asian climate," *J. Hydrometeorol.*, vol. 8, pp. 770–789, 2007.
- [3] G. Wu, Y. Liu, B. He, Q. Bao, A. Duan, and F.-F. Jin, "Thermal controls on the Asian summer monsoon," *Sci. Rep.*, vol. 2, no. 1, 2012, Art. no. 404.
- [4] T. Yao *et al.*, "Different glacier status with atmospheric circulations in Tibetan plateau and surroundings," *Nature Climate Change*, vol. 2, no. 9, pp. 663–667, 2012.
- [5] C. Kidd and G. Huffman, "Global precipitation measurement," *Meteorological Appl.*, vol. 18, no. 3, pp. 334–353, 2011.
- [6] B. Bookhagen and D. W. Burbank, "Toward a complete Himalayan hydrological budget: Spatiotemporal distribution of snowmelt and rainfall and their impact on river discharge," *J. Geophysical Res., Earth Surf.*, vol. 115, no. F3019, pp. 1–25, 2010.
- [7] Y. Ma, Y. Zhang, D. Yang, and S. B. Farhan, "Precipitation bias variability versus various gauges under different climatic conditions over the third pole environment (TPE) region," *Int. J. Climatol.*, vol. 35, no. 7, pp. 1201–1211, 2015.
- [8] G. E. Liston and K. Elder, "A meteorological distribution system for high-resolution terrestrial modeling (MicroMet)," *J. Hydrometeorol.*, vol. 7, no. 2, pp. 217–234, 2006.
- [9] C. Camera, A. Bruggeman, P. Hadjinicolaou, S. Pashiardis, and M. Lange, "Evaluation of interpolation techniques for the creation of gridded daily precipitation ($1 \times 1 \text{ km}^2$); Cyprus, 1980–2010: Gridded daily precipitation," *J. Geophysical Res. Atmospheres*, vol. 119, pp. 693–712, 2014.
- [10] H. Huang, Z. Liang, B. Li, and D. Wang, "A new spatial precipitation interpolation method based on the information diffusion principle," *Stochastic Environmental Res. Risk Assessment*, vol. 33, no. 3, pp. 765–777, 2019.
- [11] L. Zhang *et al.*, "Interpolated or satellite-based precipitation? Implications for hydrological modeling in a meso-scale mountainous watershed on the Qinghai-Tibet plateau," *J. Hydrol.*, vol. 583, 2020, Art. no. 124629.
- [12] R. Xu, F. Tian, L. Yang, H. Hu, H. Lu, and A. Hou, "Ground validation of GPM IMERG and TRMM 3B42V7 rainfall products over southern Tibetan plateau based on a high-density rain gauge network," *J. Geophysical Res. Atmospheres*, vol. 122, no. 2, pp. 910–924, 2017.
- [13] J. Qin, K. Yang, S. Liang, and X. Guo, "The altitudinal dependence of recent rapid warming over the Tibetan plateau," *Climatic Change*, vol. 97, pp. 321–327, 2009.
- [14] B. Yong *et al.*, "Global view of real-time trmm multisatellite precipitation analysis: Implications for its successor global precipitation measurement mission," *Bull. Amer. Meteorol. Soc.*, vol. 96, no. 2, pp. 283–296, 2015.
- [15] T. Dinku, E. N. Anagnostou, and M. Borga, "Improving radar-based estimation of rainfall over complex terrain," *J. Appl. Meteorol.*, vol. 41, no. 12, pp. 1163–1178, 2002.
- [16] U. Germann, G. Galli, M. Boscarelli, and M. Bolliger, "Radar precipitation measurement in a mountainous region," *Quart. J. Roy. Meteorol. Soc.*, vol. 132, no. 618, pp. 1669–1692, 2006.
- [17] A. Y. Hou *et al.*, "The global precipitation measurement mission," *Bull. Amer. Meteorol. Soc.*, vol. 95, no. 5, pp. 701–722, 2014.
- [18] G. Villarini and W. F. Krajewski, "Empirically-based modeling of spatial sampling uncertainties associated with rainfall measurements by rain gauges," *Adv. Water Resour.*, vol. 31, no. 7, pp. 1015–1023, 2008.
- [19] Y. Hong, S. Chen, X. Xue, and G. Hodges, "Global precipitation estimation and applications," in *Multiscale Hydrologic Remote Sensing: Perspectives Appl.*, N.-B. Chang and Y. Hong, Eds. CRC Press, 2012, pp. 371–386.
- [20] G. J. Huffman *et al.*, "The TRMM multisatellite precipitation analysis (TMPA): Quasi-global, multiyear, combined-sensor precipitation estimates at fine scales," *J. Hydrometeorol.*, vol. 8, no. 1, pp. 38–55, 2007.
- [21] R. Joyce, J. Janowiak, P. Arkin, and P. Xie, "CMORPH: A method that produces global precipitation estimates from passive microwave and infrared data at high spatial and temporal resolution," *J. Hydrometeorol.*, vol. 5, pp. 487–503, 2004.
- [22] S. Sorooshian, K.-L. Hsu, X. Gao, H. V. Gupta, B. Imam, and D. Braithwaite, "Evaluation of PERSIANN system satellite-based estimates of tropical rainfall," *Bull. Amer. Meteorol. Soc.*, vol. 81, no. 9, pp. 2035–2046, 2000.
- [23] T. Kubota *et al.*, "Global precipitation map using satellite-borne microwave radiometers by the GSMaP project: Production and validation," *IEEE Trans. Geosci. Remote Sens.*, vol. 45, no. 7, pp. 2259–2275, Jul. 2007.
- [24] X. Xue *et al.*, "Statistical and hydrological evaluation of TRMM-based Multi-satellite precipitation analysis over the Wangchu basin of Bhutan: Are the latest satellite precipitation products 3B42V7 ready for use in ungauged basins?," *J. Hydrol.*, vol. 499, pp. 91–99, 2013.
- [25] K. Tong, F. Su, D. Yang, and Z. Hao, "Evaluation of satellite precipitation retrievals and their potential utilities in hydrologic modeling over the Tibetan plateau," *J. Hydrol.*, vol. 519, pp. 423–437, 2014.
- [26] G. Jackson *et al.*, "The global precipitation measurement (GPM) mission for science and society," *Bull. Amer. Meteorol. Soc.*, vol. 98, pp. 1679–1695, 2016.
- [27] G. Tang, Y. Ma, D. Long, L. Zhong, and Y. Hong, "Evaluation of GPM day-1 IMERG and TMPA version-7 legacy products over mainland China at multiple spatiotemporal scales," *J. Hydrol.*, vol. 533, pp. 152–167, 2016.
- [28] A. Gebregiorgis *et al.*, "To what extent is the day-1 GPM IMERG satellite precipitation estimate improved as compared to TRMM TMPA-RT?," *J. Geophysical Res. Atmospheres*, vol. 123, pp. 1694–1707, 2018.
- [29] A. Dezfuli, C. Ichoku, K. Mohr, and G. Huffman, "Precipitation characteristics in west and east Africa, from satellite and in-situ observations," *J. Hydrometeorol.*, vol. 18, pp. 1799–1805, 2017.
- [30] R. Oliveira, V. Maggioni, D. Vila, and L. Porcaccia, "Using satellite error modeling to improve GPM-Level 3 rainfall estimates over the central amazon region," *Remote Sens.*, vol. 10, pp. 1–12, 2018, Art. no. 336.
- [31] E. Sharifi, R. Steinacker, and B. Saghaian, "Assessment of GPM-IMERG and other precipitation products against gauge data under different topographic and climatic conditions in Iran: Preliminary results," *Remote Sens.*, vol. 8, no. 2, 2016, Art. no. 135.
- [32] W. Wang, H. Lu, T. Zhao, L. Jiang, and J. Shi, "Evaluation and comparison of daily rainfall from latest GPM and TRMM products over the mekong river basin," *IEEE J. Sel. Topic Appl. Earth Observ. Remote Sens.*, vol. 10, no. 6, pp. 2540–2549, Jun. 2017.
- [33] G. Tang *et al.*, "Statistical and hydrological comparisons between TRMM and GPM level-3 products over a midlatitude basin: Is day-1 IMERG a good successor for TMPA 3B42V7?," *J. Hydrometeorol.*, vol. 17, no. 1, pp. 121–137, 2016.
- [34] D. Lu and B. Yong, "Evaluation and hydrological utility of the latest GPM IMERG V5 and GSMaP V7 precipitation products over the Tibetan plateau," *Remote Sens.*, vol. 10, no. 12, 2018, Art. no. 2022.
- [35] S. Zhang, D. Wang, Z. Qin, Y. Zheng, and J. Guo, "Assessment of the GPM and TRMM precipitation products using the rain gauge network over the tibetan plateau," *J. Meteorol. Res.*, vol. 32, no. 2, pp. 324–336, 2018.
- [36] Y. Ma *et al.*, "Similarity and error intercomparison of the GPM and its Predecessor-TRMM multisatellite precipitation analysis using the best available hourly gauge network over the Tibetan plateau," *Remote Sens.*, vol. 8, no. 7, 2016, Art. no. 569.
- [37] G. Tang, Y. Ma, D. Long, L. Zhong, and Y. Hong, "Evaluation of GPM day-1 IMERG and TMPA version-7 legacy products over mainland china at multiple spatiotemporal scales," *J. Hydrol.*, vol. 533, pp. 152–167, 2015.
- [38] J. Tan, W. A. Petersen, and A. Tokay, "A novel approach to identify sources of errors in IMERG for GPM ground validation," *J. Hydrometeorol.*, vol. 17, no. 9, pp. 2477–2491, 2016.
- [39] T. Kubota *et al.*, "Recent progress in global satellite mapping of precipitation (GSMaP) product," in *Proc. IEEE Int. Geosci. Remote Sens. Symp.*, Jul. 2017, pp. 2712–2715.
- [40] S. Chen *et al.*, "Evaluation of spatial errors of precipitation rates and types from TRMM Space-borne radar over the southern CONUS," *J. Hydrometeorol.*, vol. 14, pp. 1884–1896, 2013.
- [41] K. Taylor, "Summarizing multiple aspects of model performance in a single diagram," *J. Geophysical Res.*, vol. 106, pp. 7183–7192, 2001.
- [42] Z. Zhu, B. Yong, L. Ke, G. Wang, L. Ren, and X. Chen, "Tracing the error sources of global satellite mapping of precipitation for GPM (GPM-GSMaP) over the Tibetan plateau, China," *IEEE J. Sel. Topic Appl. Earth Observ. Remote Sens.*, vol. 11, no. 7, pp. 2181–2191, Jul. 2018.
- [43] T. Dinku, S. Chidzambwa, P. Ceccato, S. J. Connor, and C. F. Ropelewski, "Validation of high-resolution satellite rainfall products over complex terrain," *Int. J. Remote Sens.*, vol. 29, no. 14, pp. 4097–4110, 2008.
- [44] S. Shige, S. Kida, H. Ashiwake, T. Kubota, and K. Aonashi, "Improvement of TMI rain retrievals in mountainous areas," *J. Appl. Meteorol. Climatol.*, vol. 52, pp. 242–254, 2013.
- [45] A. Behrangi *et al.*, "Satellite-based precipitation estimation and its application for streamflow prediction over mountainous western U.S. basins," *J. Appl. Meteorol. Climatol.*, vol. 53, pp. 2823–2842, 2014.
- [46] G. Huffman, "Algorithm theoretical basis document (ATBD) version 4.4 for the NASA global precipitation measurement (GPM) integrated Multi-satellite retrievals for GPM (I-MERG)," NASA, pp. 1–30, 2014.

- [47] Z.-c. Hao, K. Tong, X.-l. Liu, and L.-l. Zhang, "Capability of TMPA products to simulate streamflow in Upper Yellow and Yangtze river basins on Tibetan plateau," *Water Sci. Eng.*, vol. 82, pp. 237–249, 2014.
- [48] A. M. El Kenawy, J. I. Lopez-Moreno, M. F. McCabe, and S. M. Vicente-Serrano, "Evaluation of the TMPA-3B42 precipitation product using a high-density rain gauge network over complex terrain in northeastern Iberia," *Global Planet. Change*, vol. 133, pp. 188–200, 2015.
- [49] G. Huffman, "Algorithm theoretical basis document (ATBD) Version 06 for the NASA global precipitation measurement (GPM) integrated multi-satellite retrievals for GPM (IMERG)," *NASA*, pp. 1–36, 2019.
- [50] L. Zhu, J. Liu, A.-X. Zhu, M. Sheng, and Z. Duan, "Spatial distribution of diurnal rainfall variation in summer over China," *J. Hydrometeorol.*, vol. 19, no. 4, pp. 667–678, 2018.
- [51] E. Sharifi, J. Eitzinger, and W. Dorigo, "Performance of the state-of-the-art gridded precipitation products over mountainous terrain: A regional study over Austria," *Remote Sens.*, vol. 11, no. 17, 2019, Art. no. 2018. [Online]. Available: <https://www.mdpi.com/2072-4292/11/17/2018>

Qiong Li received the Ph.D. degree in cartography and geographical information system from the University of Chinese Academy of Sciences, Beijing, China, in 2016.

She is currently a Lecturer with Qinghai University, Xining, China. Her research interests include radar quantitative precipitation estimation.

Jiahua Wei received the Ph.D. degree from the China University of Geosciences, Beijing, China, in 2001.

He is a Professor with the Department of Hydrarlic Engineering, Tsinghua University, Beijing, China, and he is also a part-time Professor with Qinghai University, Xining, China. His research interests include hydrology and water resource, hydrometeorology, and hydroinformatics.

Jianguo Yin, photograph and biography not available at the time of publication.

Zhen Qiao, photograph and biography not available at the time of publication.

Wang Peng, photograph and biography not available at the time of publication.

Haiyue Peng, photograph and biography not available at the time of publication.